Two-electron one-photon transitions into the doubly ionized K shell*

Ch. Stoller, W. Wölfli, G. Bonani, M. Stöckli, and M. Suter
Laboratorium für Kernphysik, Eidgenössische Technische Hochschule, 8093 Zürich, Switzerland
(Received 20 September 1976)

Correlated two-electron transitions into the doubly ionized K shell have been observed in Al-Al, O-Ca, Ca-Ca, Fe-Fe, Fe-Ni, Ni-Fe, and Ni-Ni collisions at beam energies between 24 and 40 MeV. In these transitions one photon carries away the entire two-electron transition energy. The cross sections for the characteristic radiation and the two-electron radiation have been determined. The measured branching ratios between the single- and double-electron transition into the doubly ionized K shell are compared with various theoretical predictions. The theoretical and experimental results are found to be in qualitative agreement.

I. INTRODUCTION

X-ray spectra measured in heavy-ion collisions at medium energies (~ 1 MeV/amu) are quite different from proton-induced spectra, both in their continuous and in their characteristic part. The characteristic lines (observed with a solid-state detector) are broadened and shifted towards higher energies.[1] The continuous part of the spectrum is different from the proton-induced spectrum in its magnitude as well as in its shape as a consequence of the quasimolecular radiation emitted in heavy-ion collisions.[2]

The broadening and the shift of the characteristic lines is caused by highly ionized states which are produced in heavy-ion collisions. The outer shells are almost completely ionized and multiple vacancies are created in the inner shells. Measurements of the K lines with a crystal spectrometer show that the characteristic lines are composed of many satellites which must be attributed to different L-shell ionization states.[3,4] There even exists a certain probability for a double ionization of the K shell. These double vacancies can be filled not only by the independent transition of two electrons (accompanied by the emission of two photons and/or Auger electrons) but also by a correlated jump of two electrons accompanied by the emission of only one photon with the total transition energy. The lines from this two-electron one-photon transition are found at approximately the double K-transition energy; such lines were observed in Al-Al, O-Ca, Ca-Ca, Fe-Fe, Fe-Ni, Ni-Fe and Ni-Ni collisions.[5] Similar results have been reported for other elements by several groups.[6,7,8]

Two-electron one-photon transitions (in the following called two-electron transitions) were predicted by Heisenberg,[9] Condon,[10] and Goudsmit and Gropper.[11] The first calculations of the probabilities of single and double excitation in He and He-like ions were done by Vinti.[12] Double excitation of He was observed a few years later in low-energy electron collisions.[13] A direct observation of double excitation in He absorption spectra was reported only in 1965 by Madden and Codling.[14]

Two-electron transitions in the outer shells of light elements are of some importance in astrophysics. Several groups have shown that the anomalous intensities of the Bowen lines in planetary nebulas can be explained assuming a two-electron transition,[15,16,17,18] the emission lines of which cannot be observed, being completely absorbed owing to their wavelength.

Åberg showed in 1971[19] that shoulders on the low-energy side of x-ray lines observed in several experiments can be explained by a two-electron transition where one electron is lifted into an upper shell and another falls into a lower shell (e.g., $1s4s$-$3p3s$). This effect is also called the radiative Auger effect (RAE).

Dow and Franceschetti predicted that two-electron transitions into the L shell should be observable.[20] A subsequent search for radiative two-electron transitions into the K shell, however, has not been successful,[21] although the Auger effect associated with the correlated two-electron transition into the L shell (i.e., an LL-MMM transition) has been found by Afrosimov *et al.*[36]

In the following we shall describe our measurements of double electron transitions into the K shell. The observed energies and branching ratios will be discussed and compared with calculations based on the model of Vinti and with recent predictions of several authors.[22,23,24,25,26]

II. EXPERIMENTAL SET-UP

Three different experimental arrangements were used, in two of which the x rays were measured with a semiconductor detector. The third setup (a crystal spectrometer) was used to resolve the satellite structure of the characteristic lines. The first two setups were mainly used to measure

molecular-orbital (MO) x rays; a large part of the two-electron data is a by-product of our measurements of MO x rays.[27,28]

With the first setup (Fig. 1) the x-ray emission cross sections in the different systems were determined. The x rays were measured at 90° with respect to the beam axis; a surface-barrier detector mounted at 45° with respect to the beam axis was used to measure the elastically scattered ions. The x-ray emission cross sections could then be determined relative to the Rutherford cross sections, i.e., the target thickness did not have to be known very precisely. This is advantageous since in heavy ion collisions the target can become thinner during the bombardment. The integrated current was also measured. This allowed us to determine the cross sections directly (if the target thickness was known). The same arrangement was used to determine the absorption coefficients of the Al absorbers used in these experiments.

Most measurements were done with a different set-up (Fig. 2), which was mainly used to determine MO x-ray anisotropies. With this arrangement the Doppler shift of projectile x rays could be measured, thus allowing us to distinguish between beam and target x rays. X rays were measured with two detectors, of which one served only as a monitor, whereas the second one could be moved to different angles with respect to the beam axis. The integrated current was measured, but not used for monitoring purposes as secondary electrons produced in the target and in the collimator could disturb the measurement (although a suppressor voltage was applied to the collimator). The chamber was provided with 20-μm Al x-ray windows. The target angle was chosen in such a way that self-absorption was the same for both detector angles used in the experiment. The third setup (Fig. 3) was used to study the satellite

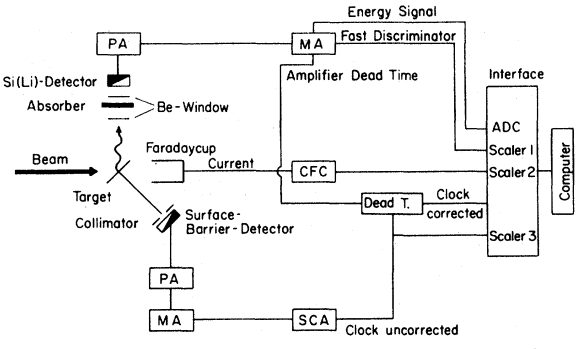

FIG. 1. Experimental set-up which was used to determine x-ray cross sections PA, preamp; MA, main amplifier; CFC, current-frequency converter; SCA, single-channel analyzer.

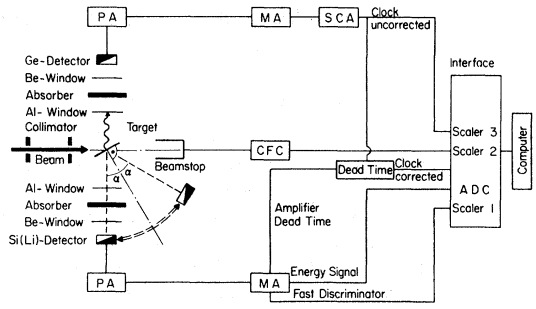

FIG. 2. Set-up used to measure x-ray angular distributions. The Ge detector was used as a monitor; 20-μm Al foils were used as x-ray windows.

and hypersatellite structure of the characteristic lines. For this purpose a flat crystal Bragg spectrometer was used with a flow proportional counter as an x-ray detector. The goniometer was driven by a computer-controlled step-motor. The integrated current (i.e., the pulses from the current-to-frequency converter) was used for monitoring. The following crystals were used: LiF (200) ($2d$ = 4.0276 Å) for the Ca, Fe, and Ni measurements and EDDT ($2d$ = 8.808 Å) for the Al measurements.

III. RESULTS

A. Emission cross sections for the characteristic radiation

All cross sections in the observed spectra were determined relative to the $K\alpha$ cross sections. The latter had to be measured. This was done for the following systems: Ca-Ca, Fe-Fe, Fe-Ni, Ni-Fe, and Ni-Ni; in the O-Ca case a thick metallic Ca target was used.

The negative ions produced in a Middleton ion source were accelerated in the EN-tandem to energies between 24 and 40 MeV. Thin foils were used as targets: 20 μg/cm^{2}Ca on C backing, 25 μg/cm^{2}Fe on C backing and 70 μg/cm^{2}Ni (self-supporting). The projectile x-ray production in the backing could be shown to be negligible. Average cross sections were also determined for the thick targets (200–400 μg/cm^2) which were used

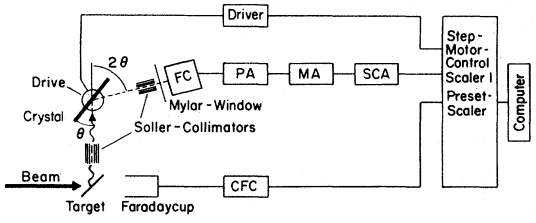

FIG. 3. Computer-controlled crystal spectrometer. The flow counter (FC) used to measure the x-rays was provided with a 12-μm Mylar window.

for the determination of the two-electron one-photon transition. In the thin foil cases the cross sections could be determined with respect to the Rutherford cross sections. In the "thick" target cases a properly averaged Rutherford cross section or the integrated current had to be used.

The cross sections were measured with beam currents between 0.1 and 1.5 nA (charge states were 4^+ to 6^+) in order to keep the x-ray count rate below 4000 cps (i.e., the main amplifier dead time was smaller than 40%). The x-ray count was properly corrected for absorption (windows, air) and detector efficiency (gold layer, dead layer, escape lines).

The cross sections are compiled in Table I together with the two-electron cross sections, which will be discussed in the next section. The relatively large differences of the Fe and Ni cross sections in the slightly asymmetric systems Fe-Ni and Ni-Fe can be explained by the theory of "vacancy sharing".[29]

TABLE I. Cross sections for the characteristic radiation ($K\alpha$) and the two electron transitions observed in various systems. For Cl-Ni, the Ni $K\alpha\alpha$ line could not be observed because of the large MO x-ray background.

Projectile-Target	E_{lab} (MeV)	$\sigma(K\alpha)$ (b)	$\sigma(K\alpha\alpha)$ (mb)	$\sigma(K\alpha\beta)$ (mb)
Ca Ca	40	11 150 ± 600	65 ± 12	< 10
Ca Ca	25	4 400 ± 400	21 ± 5	< 4
Fe Fe	40	6 200 ± 300	19 ± 1	3 ± 1
Fe Fe	25	2 860 ± 200	3.0 ± 0.4	< 0.4
Ni Ni	40	3 800 ± 250	4.0 ± 0.7	0.8 ± 0.5
Ni Ni	24	1 430 ± 150	0.6 ± 0.15	< 0.15
Fe Ni	40	3 100 ± 200 1 800 ± 200	9.3 ± 2.0 1.6 ± 0.5	1.9 ± 1.0 < 0.3
Fe Ni	25	1 570 ± 120 600 ± 80		
Ni Fe	40	1 380 ± 100 3 350 ± 200	1.2 ± 0.4 13.5 ± 2.0	< 0.3 4.0 ± 1.3
Ni Fe	24	550 ± 70 1 800 ± 150		
Cl Ni	40	48 000 ± 2 000 660 ± 60		
Cl Ni	25	7 570 ± 700 56 ± 10		

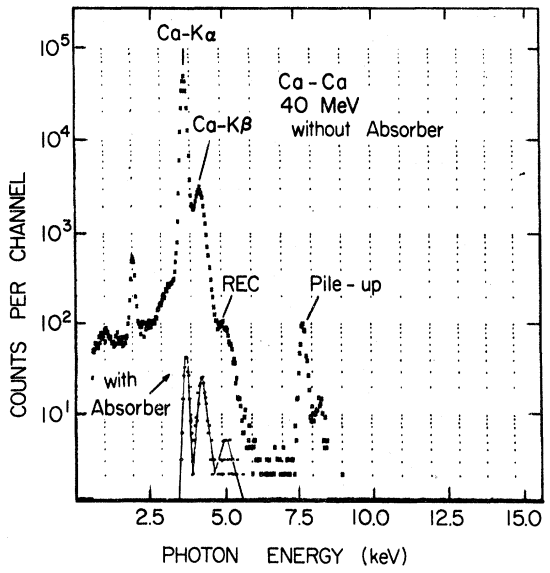

FIG. 4. Ca-Ca x-ray spectra measured with a 30 mm^2, 3-mm-thick Si(Li) detector (resolution 165 eV at 5.9 keV) at 40-MeV beam energy without and with an absorber of 80-μm Al (solid line). Both spectra are normalized to the same number of elastically scattered Ca ions.

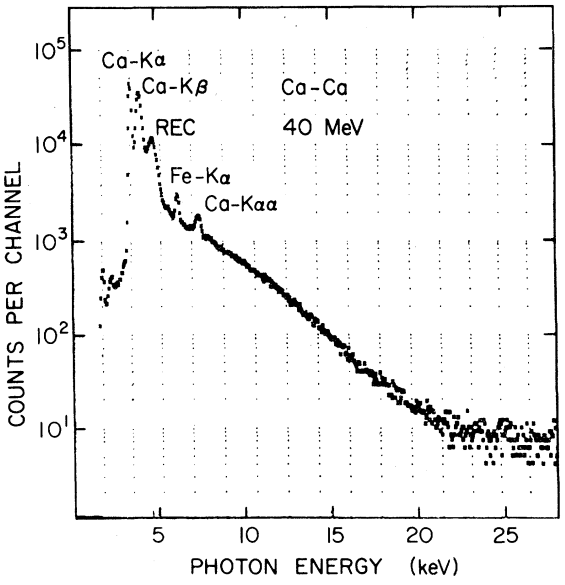

FIG. 5. Ca-Ca spectrum (same as lower curve in Fig. 4, with 80-μm Al absorber) including the high-energy part of the spectrum. The line denoted by Ca $K\alpha\alpha$ is due to the correlated two-electron transition. The peak Fe $K\alpha$ is caused by iron impurity, whereas the REC peak reflects radiative electron capture. The continuum in the high-energy range indicates transitions between quasimolecular Ca-Ca states formed transiently during collision time.

B. Analysis of the two-electron one-photon lines

During the measurements of the $K\alpha$ cross sections no unusual x-ray lines were observed. This can be seen from the Ca-Ca spectrum shown in Fig. 4. Besides the characteristic lines one finds two escape lines, a broad "line" caused by REC,[30] and the $K\alpha+K\alpha$, $K\alpha+K\beta$ pileup lines.

A spectrum measured with an 80-μm Al-absorber looks completely different (Fig. 5). The characteristic $K\alpha$ radiation was attenuated by a factor $\sim 10^4$. Two additional lines can be observed, whereas the pileup lines vanish because of the decreased count rate (40 cps against 2000 cps). One line is caused by an iron contamination of the target, the second one ($K\alpha\alpha$) must be attributed to a Ca double-electron transition.

In all cases reported here, one or two double-electron peaks were observed, either from a K^2-L^2 ($K\alpha\alpha$) or from a K^2-LM ($K\alpha\beta$) transition. The energies of the x-ray transitions could be determined quite accurately. They are compiled in Table II. In all cases the $K\alpha\alpha$ lines are shifted by about 100–160 eV with respect to twice the $K\alpha$ energy (pileup line). This displacement can be explained by the reduced screening of the doubly ionized K shell.

As the double-electron line is very weak compared with the characteristic radiation, several other effects which might lead to similar peaks had to be ruled out: random pileup, "true" pileup, target impurities, Coulomb excitation, and secondary excitation.

The problem of random pileup has been considered in detail.[28] The pileup rejector used had a pulse-pair resolution of 1.5 μsec, i.e., two pulses

TABLE II. Energies of the observed x-ray transitions measured with the Si(Li) detector. The third column gives the x-ray energies for the case of no additional outer-shell vacancies as can be found in Ref. 35.

Projectile-Target	Energy (MeV)	$E(K\alpha)$ theor. (keV)	$E(K\alpha)$ exp. (keV)	$E(K\alpha\alpha)$ (keV)	$E(K\alpha\beta)$ (keV)
Ca Ca	40	3.691	3.814 ± 0.010	7.660 ± 0.030	
Ca Ca	25	3.691	3.784 ± 0.010	7.637 ± 0.010	
Fe Fe	41.5	6.400	6.475 ± 0.005	13.075 ± 0.035	13.850 ± 0.050
Fe Fe	25	6.400	6.477 ± 0.010	13.050 ± 0.030	
Ni Ni	40	7.477	7.535 ± 0.005	15.230 ± 0.010	16.170 ± 0.040
Ni Ni	24	7.477	7.520 ± 0.007	15.200 ± 0.040	
Fe Ni	41.5	6.400 7.477	6.467 ± 0.007 7.536 ± 0.007	13.090 ± 0.020 15.250 ± 0.050	13.920 ± 0.060
Fe Ni	25	6.400 7.477	6.455 ± 0.010 7.525 ± 0.010		
Ni Fe	40	7.477 6.400	7.533 ± 0.004 6.470 ± 0.003	15.220 ± 0.020 13.090 ± 0.015	13.870 ± 0.050
Ni Fe	24	7.477 6.400	7.512 ± 0.010 6.467 ± 0.010		
Cl Ni	40	2.622 7.477	2.753 ± 0.015 7.545 ± 0.010		
Cl Ni	25	2.622 7.477	 7.532 ± 0.006		
O Ca	30	3.691	3.752 ± 0.007	7.592 ± 0.020	
Al Al	25	1.486	1.520 ± 0.010	3.180 ± 0.020	

arriving within 1.5 μsec are observed as one pulse with the same total energy. Since the pileup peaks of the $K\alpha$ lines lie very close to the expected $K\alpha\alpha$ lines, this effect must be reduced to a negligible amount. This is achieved when the characteristic lines are attenuated by several orders of magnitude (see Fig. 4) using appropriate Be or Al absorbers, and the count rate is kept below 100 cps. In our experiment, an 80-μm Al absorber was used in the case of Ca-Ca and 720-μm Al in that of Ni-Ni.

"True" pile-up could also be ruled out, i.e., the probability that both x rays emitted in a two-electron two-photon transition are observed simultaneously in the detector is orders of magnitude to small to explain the observed effect. This small probability is due to the small solid angle of the detector and to the strong attenuation of characteristic x rays (~10^4–10^6). It should be noted that only about 1% of the observed characteristic x rays can be attributed to a transition into the doubly ionized K shell.

All targets were checked for impurities with the highly sensitive proton induced x-ray analysis.[28] The impurities in the targets cannot explain the observed lines. Measurements under different angles with respect to the beam axis showed that a part of the x rays must come from the projectile. In the symmetric cases the $K\alpha\alpha$ line is split, when observed under 30°, in asymmetric cases the projectile lines are shifted (see also Ref. 7), as can be seen in Fig. 6.

Coulomb excitation cannot have caused the observed lines as there are no known γ lines in the energy range of interest.

To exclude secondary excitation of x rays in the windows or in the absorber only high-purity Al was used as an absorber (except in the Al-Al measurements, where a Be absorber was used); the used collimator also consisted of high purity Al. The observed lines cannot be explained by Au L lines produced in the detector gold layer. Note also that such lines should not be influenced by the detector angle.

C. Determination of the hypersatellite lines

The x-ray lines associated with single-electron transitions into the doubly ionized K shell are called hypersatellites. They will be denoted by $K\alpha^h$ and $K\beta^h$ in this paper. This effect was observed first by Catterall and Trotter in the x-ray spectra of Li and Be.[31]

To determine the $K\alpha^h$ to $K\alpha$ ratio precisely a crystal spectrometer must be used, because the resolution of a solid-state detector is not sufficient (in the case of the elements investigated here) to resolve the small $K\alpha^h$ line from the adjacent

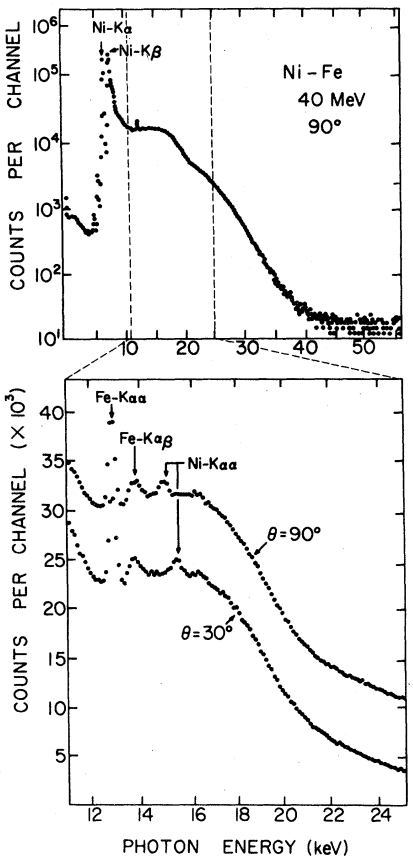

FIG. 6. Spectrum from Ni-Fe collisions at 40 MeV. The lower part of the figure shows the two-electron peak in a linear scale. The Doppler shift caused by the projectile motion is clearly visible.

$K\alpha$ and/or $K\beta$ lines. In Si(Li) spectra the hypersatellite can only be determined through the slight asymmetry of the characteristic lines. This determination is very difficult because the precise shape of the characteristic lines is not known (unresolved satellites).

An exact knowledge of the ratio between the "normal" $K\alpha$ transition and the $K\alpha^h$ line is necessary if the branching ratio between the hypersatellites and the correlated transitions has to be determined. From the measurements with solid-state detectors, only the ratio between the characteristic lines and the correlated jump is known. The branching ratio then had to be determined from two separate experiments. Firstly the $K\alpha$ to $K\alpha\alpha$ ratio was measured with a solid-state detector and secondly the $K\alpha$ to $K\alpha^h$ ratio was determined with a crystal spectrometer. Figure 7 shows a Fe-Fe spectrum measured with a solid-state detector (upper half) and the part of the spectrum measured with a crystal spectrometer using a LiF(200) crystal as an analyzer.

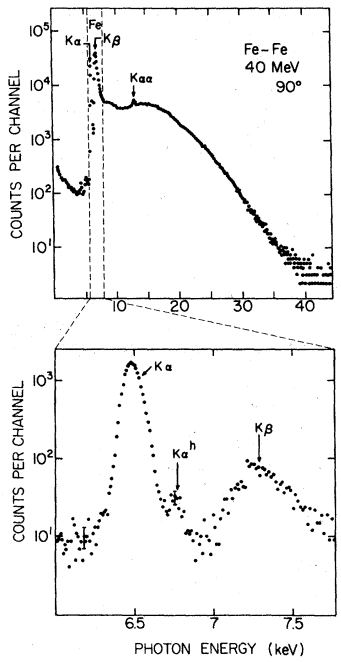

FIG. 7. Spectra measured in Fe-Fe collisions (40 MeV). The upper half shows the spectrum measured with a solid-state detector. The spectrum observed with the crystal spectrometer is shown in the lower part. The hypersatellite line ($K\alpha^h$) is clearly visible. The observed lines are broader than the instrumental resolution.

The observed $K\alpha$ to $K\alpha^h$ intensity ratios are compiled in Table III. The ratios decrease from 2% (Al-Al) to 0.5% (Ni-Ni). The fact that the Ni $K\alpha^h$ line was quite weak rendered its determination quite difficult, as the resolution was also worst for this case (~60-eV FWHM). Better resolution might be achieved in the present set-up by using an analyzing crystal with a smaller spacing such as LiF(220) with $2d = 2.85$ Å instead of 4.0276 Å for LiF(200). The energies of the $K\alpha$ and $K\alpha^h$ lines are shown in Table III. The observed differences $E(K\alpha^h) - E(K\alpha)$ agree well with calculations of Nagel *et al.*[21]

In Al and Ca, not only the hypersatellite lines but also the satellite lines (from different L-shell ionization states) could be resolved (see Fig. 8). A discussion of these spectra can be found in Refs. 3, 4, and 28.

In the Ni and Fe spectra the satellite lines could not be resolved. This is not only a consequence of the worse energy resolution but also of the fact that many different M-shell ionization states are found here, whereas in Al and Ca the M shell was almost completely ionized. This leads to a broadening of the satellite lines, which cannot be resolved any longer. Therefore a broad peak is observed (much broader than the experimental resolution).

D. Theoretical considerations

Until recently practically no calcuation of two-electron transition energies and transition rates existed. The only work dealing with K-shell two-electron transitions was done by Vinti in 1932.[12] He considered the probabilities of two-electron one-photon excitation in He and He-like ions. The wave functions which are due to Eckart[32] are products of H-like wave functions, where the nuclear charge Z is replaced by a free parameter.

The following ground-state ($1s^2$) wave function was assumed:

$$\Phi_{1s^2} = \frac{1}{\sqrt{2}\,(1+c^2)^{1/2}} \times [\psi_{1s}(1,\gamma)\psi_{1s}(2,\delta) + \psi_{1s}(1,\delta)\psi_{1s}(2,\gamma)],$$

$$c = \int \psi_{1s}(1,\gamma)\psi_{1s}(1,\delta)\,d\tau = 8\,(\sqrt{\gamma}\sqrt{\delta}/\gamma\delta)^3.$$

For the doubly excited state, a $2s2p$ state is assumed. Note that neither the $2s^2$ nor the $2p^2$ state can decay to the ground state by an $E1$ transition.

The wave function for the $2s2p$ state is

$$\Phi_{2s2p} = (1/\sqrt{2})[\psi_{2s}(1,Z)\psi_{2p}(2,\beta) + \psi_{2s}(2,Z)\psi_{2p}(1,\beta)].$$

The parameters β, γ, δ have to be determined minimizing the binding energies of the respective states. The energies determined from these wave functions compare well with the calculations of Betz[22] (if the relativistic correction to the binding energy is taken into account). The energies are shown in Table IV.

To determine the branching ratio $N(K\alpha^h)/N(K\alpha\alpha)$, i.e., the ratio between the single-electron and the double-electron radiative transition rates, both matrix elements have to be calculated. The hypersatellite matrix element is practically equal to the "normal" $1s^2$-$1s2p$ matrix element. For the calculation of the transition rate only the larger transition energy has to be taken into account. The branching ratios determined from this calculations are compatible with our data. They are somewhat larger than branching ratios calculated by Åberg *et al.*,[24] with more sophisticated Hartree-Fock calculations.

The formulas show that the branching ratio increases approximately like Z^2. The matrix element of the correlated transition,

$$m_{fi}^{\alpha\alpha} = \langle 1s^2 | \vec{r} | 2s2p \rangle$$

is proportional to Z^{-2}, whereas the hypersatellite

TABLE III. X-ray intensity ratio of single-electron transitions in the singly and doubly ionized K-shell $[N(K\alpha)/N(K\alpha^h)]$. This ratio is not necessarily equal to the ratio between single- and double-vacancy production, since the fluorescence yield of each state need not be the same. The observed $K\alpha$ and $K\alpha^h$ energies are also compiled. The given $K\alpha$ energy is the average value of the observed satellite energies. In Fe and Ni the satellite lines could not be resolved. In most cases more than one hypersatellite line could be distinguished. The theoretical differences $\Delta E = E(K\alpha^h) - E(K\alpha)$ were taken from Ref. 34.

Projectile-Target	Energy (MeV)	Ratio $N(K\alpha)/N(K\alpha^h)$	$E(K\alpha^h)$ (eV)	$E(K\alpha)$ (eV)	ΔE (eV)	ΔE Theor.
Al	25	60±10	1648±3 [a]	1513±3	135±3	130
Al			1668±1 [a]		155±3	
			1684±5 [a]		171±4	
O	30	180±22	3916±3	3752±4	164±5	200
Ca			3940±3		188±5	
			3964±3		212±5	
Fe	40	82±10	6681±25	6468±5	213±25	263
Fe			6732±20		264±22	
			6761±25		293±25	
Fe	40	79±8	6687±25	6475±8	212±25	263
			6743±30		268±30	
Ni		>110	7747±25	7558±7	209±25	283
Ni	40	>100	7747±25	7535±7	212±25	283
			7842±30		307±30	
Fe		60±5.5	6725±25	6480±10	245±25	
			6766±30		286±30	
Ni	40	188±30	7795±25	7535±7	260±25	283
Ni						

[a] The Al $K\alpha^h$ lines cannot be identified unambiguously because they are superimposed on the $K\beta$ lines.

matrix element

$$m_{fi}^h = \langle 1s2s \,|\, \vec{r} \,|\, 2s2p \rangle$$

decreases only like Z^{-1}.

The increase of the branching ratio with increasing Z simply reflects the fact, that the electron-nucleus interaction increases faster (proportional to Z^2) than the electron-electron interaction (proportional to Z).

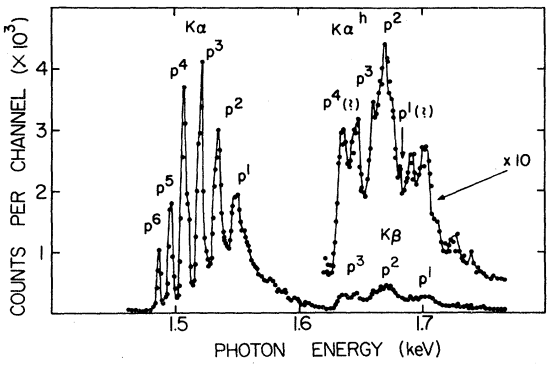

FIG. 8. Al-Al spectrum measured with the crystal spectrometer. The satellite lines corresponding to the different L-shell ionization states are well resolved. The number of the remaining $2p$ electrons is given for all lines. The hypersatellite ($K\alpha^h$) lines are superposed on the $K\beta$ lines.

IV. DISCUSSION

The observed energies have been compiled in the preceding sections. A comparison with cal-

TABLE IV. Energies for the $1s^2$-$2s2p$ transition in He-like ions, calculated from Vinti's theory. Relativistic corrections to the binding energy were taken into account. For comparison values calculated by Betz *et al.* (Ref. 22), for the $1s^2$-$2s^2$ transition increased by the $2s^2$-$2s2p$ energy difference (about 70 eV) and Madden *et al.* (Ref. 14) are shown.

Element	$E(K\alpha\alpha)$ (eV) Vinti	Betz	Madden
He	57	60.269 [a]	60.135±0.015
Al	3270		
Ca	7950		
Fe	13 580	13 646	
Ni	15 820	15 876	

[a] Calculations of Burke and McVicar (Ref. 33).

culations of different authors is given in Table V. Since the double-electron lines were not measured with the crystal spectrometer—because of the low intensity—the two-electron satellite lines could not be resolved. A precise state assignment is thus not possible. Good agreement was also found with the calculations of Hodge[25] and Nussbaumer.[23] The observed energies indicate that in Fe and Ni the most important contribution comes from ions with a closed L shell or with one L vacancy. The calculations of Hodge are not consistent with those of Betz *et al.*[22] in their absolute values (see Table V) though both authors used relativistic Hartree-Fock computer codes. From Hodge's calculations one concludes that one or two vacancies are present in the initial state. From the energies calculated by Nussbaumer one would conclude that the transitions are mostly from a closed L shell,

TABLE V. Theoretical transition energies for several configurations of Fe and Ni calculated by Betz (Ref. 22), Hodge (Ref. 25) and Nussbaumer (Ref. 23). Measured energies are given in the last column. Note that Hodge assumed that the outer shells were filled.

Configuration			Calculated energies (keV)			Exp. energies [a] (keV)
K	L	M	Betz	Nussbaumer	Hodge	
				I. Fe		
1	224		6.445		6.406	
2	223					
1	223		6.479	6.492	6.433	6.470 ± 0.003
2	222					
1	222		6.515		6.462	
2	221					
1	211		6.595			
2	21					
1	101		6.679	6.680		
2	1					
0	224		13.032	13.080	12.985	
2	123					
0	223		13.098		13.055	13.090 ± 0.015
2	122					
0	224 [b]		13.138	13.206	13.114	
2	222					
				II. Ni		
1	224		7.528		7.481	7.535 ± 0.004
2	223					
1	223		7.566	7.579	7.512	
1	222					
1	222		7.605		7.543	
2	221					
1	211		7.693			
2	21					
1	101		7.784	7.785		
2	1					
0	224		15.205	15.290	15.146	15.220 ± 0.020
2	123					
0	223		15.275		15.223	
2	122					
0	224 [b]		15.326	15.404	15.291	
2	222					

[a] The experimental energies are from the Ni-Fe (40 MeV) measurements.
[b] $E2$ transition.

TABLE VI. Theoretical and experimental branching ratios of radiative single- and double-electron transitions into the doubly ionized K shell. The theoretical values are taken from Refs. 23 and 37 and from calculations using the approach of Vinti. Kelly (Ref. 26) predicts for the Fe atom a ratio of 5630 in the dipole-length and 5860 in the dipole-velocity approximation.

Projectile-Target	Exp.	Vinti	$N(K\alpha^h)/N(K\alpha\alpha)$ Nussbaumer [a] ($E1$)	($E2$)	Gavrila and Hansen
Al Al	965 ± 180	1250			682
O Ca	2570 ± 380	3000			1240
Fe Fe	3950 ± 500	5100	2.4×10^5	1.1×10^5	1870
Fe Ni	4210 ± 430 < 11 500	5100 5800	2.4×10^5 2.5×10^5	1.1×10^5 1.2×10^5	1870 2120
Ni Fe	< 10 500 4100 ± 400	5800 5100	2.5×10^5 2.4×10^5	1.2×10^5 1.1×10^5	2120 1870
Ni Ni	5000 ± 600	5800	2.5×10^5	1.2×10^5	2120

[a] Nussbaumer's calculations give the surprising result that $E2$ transitions are more probable than $E1$ transitions for a $2s^22p^6$ initial state.

as the calculated energies are larger than those calculated by Betz *et al.* It is not possible to rule out one of the calculations since the L ionization states are not known.

The apparent discrepancy between our measurements and calculations by Nagel[34] can be explained by the fact that he assumed a $1s^2$-$2p^2$ ($E2$) transition whereas one would expect a $1s^2$-$2s2p$ ($E1$) transition, though the calculations of Nussbaumer show that the $E2$ transitions might be dominant.[23]

The comparison of the theoretical and the experimental branching ratios compiled in Table VI shows that qualitative agreement can be achieved. Until recently calculations have been based on the model of Vinti.[12] There are now calculations by Åberg *et al.*[24] based on a "shake down" model, which is not essentially different from Vinti's approach. Åberg *et al.* used more accurate wave functions obtained from Hartree-Fock calculations. Similar calculations were also performed by Gavrila and Hansen.[37] These results do not show the same Z dependence as those of Refs. 12 and 24.

The only calculations that take electron-electron correlations explicitly into account are those of Kelly[26] and Nussbaumer,[23] but the calculation of Nussbaumer disagrees by a factor of about 20 with our measurements. The cause of this discrepancy is not yet clear. The calculation of Kelly for Fe—also shown in Fig. 9—agrees fairly well with the measured value.

The theories of Åberg *et al.* and Vinti show the same Z^2 dependence of the branching ratio though their absolute values are different (Fig. 9). A comparison of the theoretical and the measured values shows that best agreement is achieved with Vinti's theory. This agreement might be fortuitous, i.e., different inaccuracies in the approximation used might cancel when the matrix element is calculated.

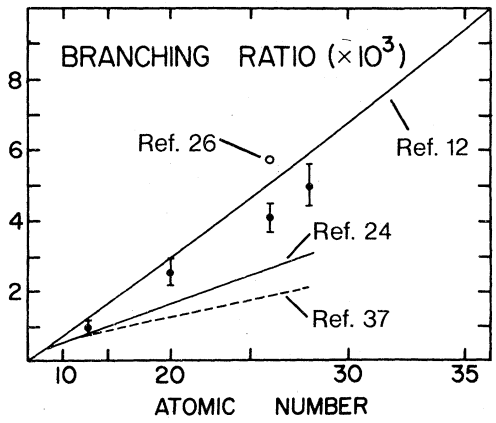

FIG. 9. Comparison of measured and calculated branching ratios. The atomic number Z is displayed in a quadratic scale. The theoretical predictions are due to Vinti (Ref. 12), Kelly (Ref. 26), Åberg *et al.* (Ref. 24) and Gavrila and Hansen (Ref. 37).

V. CONCLUSION

Correlated and uncorrelated two-electron transitions were measured in Al, Ca, Fe, and Ni. The measured energies are compatible with theoretical predictions, though the assignment of the L-ionization state gives problems. In any case, the observed energies indicate that the deexcitation occurs through an electric dipole transition.

The observed branching ratios are consistent with predictions based on the model of Vinti, as well as with the recent calculations by Åberg *et al.*[24] The Z^2-law predicted by both theories seems to be reproduced by our data, although the absolute values agree only up to a factor of 2. Perhaps detailed calculations which take configuration interaction into account explicitly will give better agreement, although the first calculations done by Nussbaumer disagree considerably with our measurements.

Theoretical calculations might be easier for lighter systems, where the electron-electron interaction is more important. But in lighter systems experimental difficulties in determining the branching ratios might become a major problem.

Measurements with heavier systems might be used to test the Z^2 law in a broader range. This is probably beyond the possibilities of an EN-Tandem, because the two-hole production rate will be insufficient to produce enough two-electron transitions so that they can be resolved from the large quasimolecular background.

Note added in proof. Most recently Knudson *et al.*[38] measured the branching ratio on Ar. Their result also agrees fairly well with the theoretical predictions. The observed energy shifts of the $K\alpha\alpha$ lines relative to twice the $K\alpha$ energies in the region from $Z = 12$ to 26 are consistent with our data.

ACKNOWLEDGMENTS

The authors would like to acknowledge stimulating discussions with Professor J. Lang and Dr. M. Simonius who also drew our attention to the existence of the effect discussed above.

---

*Work supported by the Swiss National Science Foundation.

[1]P. Richard, I. L. Morgan, T. Furuta, and D. Burch, Phys. Rev. Lett. 23, 1009 (1969).
[2]W. E. Meyerhof, T. K. Saylor, S. M. Lazame, W. A. Little, B. B. Tripplett, and L. F. Chase, Phys. Rev. Lett. 30, 2179 (1973).
[3]A. R. Knudson, D. J. Nagel, P. G. Burkhalter, and K. L. Dunning Phys. Rev. Lett. 26, 1149 (1971).
[4]J. McWherter, J. Bolger, C. F. Moore, and P. Richard, Z. Phys. B 6, 2468 (1973).
[5]W. Wölfli, Ch. Stoller, G. Bonani, M. Suter, and M. Stöckli, Phys. Rev. Lett. 35, 656 (1975).
[6]Th. P. Hoogkamer, P. Woerlee, F. W. Saris, and M. Gavrila, J. Phys. B 9, L145 (1976).
[7]R. Schuch, H. Schmidt-Böcking, R. Schulé, G. Nolte, I. Tserruya, W. Lichtenberg, and K. Stiebing, Contributed Paper Second International Conference on Inner Shell Ionization Phenomena, Freiburg, 1976, p. 161.
[8]S. M. Schafroth (private communication).
[9]W. Heisenberg, Z. Phys. 32, 841 (1925).
[10]E. U. Condon, Phys. Rev. 36, 1121 (1930).
[11]S. Goudsmit and L. Gropper, Phys. Rev. 38, 225 (1931).
[12]J. P. Vinti, Phys. Rev. 42, 632 (1932).
[13]P. Whiddington and H. Priestly, Proc. R. Soc. A 145, 462 (1934).
[14]R. P. Madden and K. Codling, Astron. Phys. J. 141, 364 (1965).
[15]J. Désequelles, Ann. Phys. (Paris) 6, 71 (1971).
[16]J. A. Kernhan, A. L. Livingston, and E. H. Pinnington, Can. J. Phys. 52, 1895 (1974).
[17]M. C. Buchet-Poulizac, thesis (Univ. de Lyon, France, 1974) (unpublished).
[18]H. Nussbaumer, Astron. Phys. Lett. 4, 183 (1969); Astron. Phys. J. 170, 93 (1971).
[19]T. Åberg, Phys. Rev. A 4, 1735 (1971).
[20]J. Dow and P. R. Franceschetti, Phys. Lett. 50A, 1 (1974).
[21]D. J. Nagel, A. R. Knudson, and P. G. Burkhalter, J. Phys. B 8, 2779 (1975).
[22]H. D. Betz and W. Wölfli, Phys. Rev. Lett. 37, 61 (1976); and H. D. Betz, Contributed Paper Second International Conference on Inner Shell Ionization Phenomena, Freiburg, 1976, p. 155.
[23]H. Nussbaumer, J. Phys. B 9, 1757 (1976).
[24]T. Åberg, K. A. Jamison, and P. Richard, Phys. Rev. Lett. 37, 63 (1976).
[25]B. Hodge (unpublished).
[26]H. P. Kelly, Phys. Rev. Lett 37, 386 (1976).
[27]W. Wölfli, Ch. Stoller, G. Bonani, M. Suter, and M. Stöckli, Proceedings of the Second International Conference on Inner Shell Ionization Phenomena, Freiburg, 1976, p. 272.
[28]Ch. Stoller, thesis (ETH, Zürich, 1976) (unpublished).
[29]K. Taulbjerg, J. Vaaben, and B. Fastrup, Phys. Rev. A 12, 2325 (1975).
[30]H. W. Schnopper, H. D. Betz, J. P. Delvaille, K. Kalata, and A. R. Sohval, Phys. Rev. Lett. 29, 898 (1972).
[31]J. A. Catterall and J. Trotter, Philos. Mag. 3, 1424 (1958).
[32]C. Eckart, Phys. Rev. 36, 878 (1930).
[33]P. G. Burke and D. D. McVicar, Proc. Phys. Soc. 86, 989 (1965).
[34]D. J. Nagel, P. G. Burkhalter, A. R. Knudson, and K. W. Hill, Phys. Rev. Lett. 36, 164 (1976).
[35]J. A. Bearden, Rev. Mod. Phys. 39, 78 (1967).
[36]V. V. Afrosimov, Yu. S. Gordeev, A. N. Zinoviev, D. H. Rasulov, and A. P. Shergin, *Electronic and Atomic Collisions, Abstracts of the Papers of the Ninth International Conference on the Physics of Elec-*

tronic and Atomic Collisions, edited by J. S. Risley and R. Geballe (University of Washington Press, 1975), p. 1068; and Zh. Eksp. Teor. Fiz., Pisma Red. 21, 535 (1975) [JETP Lett. 21, 249 (1975)].

[37]M. Gavrila and J. E. Hansen, Phys. Lett. 58A 158 (1976).

[38]A. R. Knudson, K. W. Hill, P. G. Burkhalter, and D. J. Nagel, Phys. Rev. Lett. 37, 679 (1976).